2.6 Membrane Elasticity and Morphology -

Lit:
- de Gennes and Prost "The Physics of Liquid Crystals"
- Israelachvili "Intermolecular + Surface Force" Part 3
- H. P. Duwe et al "Bending elastic moduli of lipid bilayers" J. Phys. France 51 (1990) 945-962
- J. Käs and E. Sackmann "Shape transitions and shape stability of giant phospholipid vesicles in pure water"

Self assembly of lipid bilayers

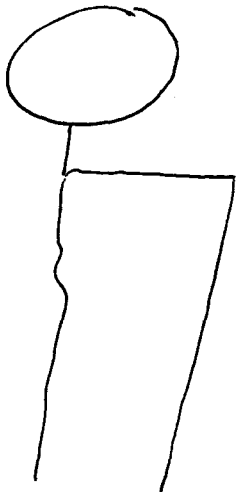

hydrophilic headgroup

fatty acids, hydrophobic due to iceberg effect

show fig page 344

show fig page 381

show fig page 386

show fig page 388

Hydrophobic Effect:

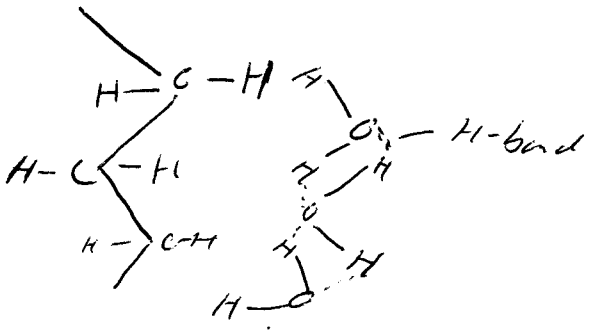

When a hydrocarbon molecule is surrounded by water, the H_2O molecules form a clathrate cage. As a result of this acquisition of structure, the entropy of water decreases, so the disposal of the hydrocarbon into the water is entropy-opposed.

Membrane Elasticity

- cell membrane are 2-dimensional fluids that adopt to any shape without any defects that could lower the ~~quality~~ quality of the membrane as a barrier!
- no surface tension ⇒ hydrophilic heads point to the outside
- no shear elasticity ⇒ fluid bilayer

- bending elasticity:

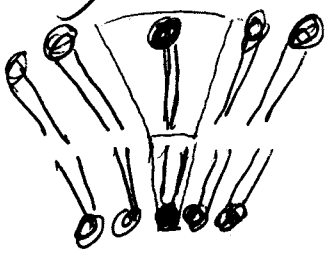

Helfrich:

$$E_{bend} = \int_{Amembrane} \left[\frac{1}{2} K_c \left(\frac{1}{r_1} + \frac{1}{r_2} \right)^2 + \gamma \right] dA$$

- K_c: bending modulus
- harmonic potential
- r_1, r_2: principal radii of curvature
- γ: compensates for spontaneous curvature

~~- Bending elasticity~~

- measuring the bending modulus
  (→ Lemmon and Brochard 1975)

show fig 1

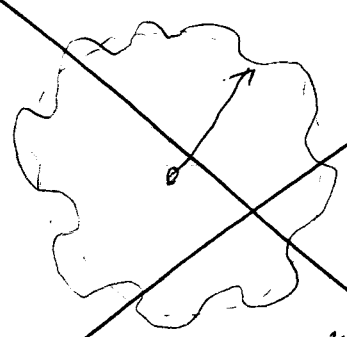

Fourier transform

$$r(\varphi, t) = r_0 \sum_{q=0}^{q_{max}} v_q(t) \, e^{-iq\varphi}$$

with $v_q(t) = \frac{1}{i\pi} \sum_{l=q,m}^{l_{max}} a_{l,m}(t) \cdot \int_0^{2\pi} Y_{l,m}\left(\frac{\pi}{2}, \varphi\right) e^{iq\varphi} \, d\varphi$

⇒ mean square of the contour fluctuations:

$$\langle |v_q(t)|^2 \rangle =$$

- measuring the bending modulus
  (→ Lennon and Brochard 1975)
  show fig 1

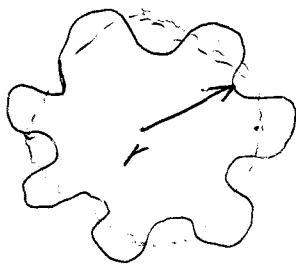

$$r(\vartheta, \varphi, t) = r_0 \left(1 + \sum_{\substack{l=0 \\ l=2}}^{\infty} a_{l,m}(t)\, Y_{l,m}(\vartheta, \varphi)\right)$$

expansion in spherical harmonics

molecular and optical cut off

$$\langle E_{bend}(t) \rangle = \int_A \left(\frac{1}{2} K_c \langle r(\vartheta, \varphi, t)^2 \rangle + \underbrace{p}_{\approx 0} \right) dA$$

for each mode: $\langle E_{bend\,l,m}(t) \rangle = \frac{1}{2} K_c (l+2)(l-1)[l(l+1)] \frac{\langle |a_{l,m}|^2 \rangle}{r_0^2}$

$$\uparrow = \frac{1}{2} k_B T$$

equipartition theorem

$$\Rightarrow \quad \langle |a_{l,m}|^2 \rangle = \frac{r_0^2 k_B T}{K_c\, l(l+1)(l+2)(l-1)}$$

$\langle |a_{l,m}|^2 \rangle$: measure; denominator: calculate

- typical values for K_c:

  DMPC $\quad K_c \approx 20\, k_B T$

  DMPC + 20% Cholesterol $\quad K_c \approx 40 k_B T$

  Erythrocytes $\quad K_c \approx 6 k_B T$

Membrane Morphology

- cytoskeleton dominates
- vesicle shape:

shape is determined by minimum of bending elasticity:

$$E_{bend} = \frac{1}{2} k_c \int \left(\frac{1}{r_1} + \frac{1}{r_2}\right)^2 dA^{in}$$

(A^{in}: inner monolayer)

constraints: ① reduced volume:

$$v := \frac{V}{\frac{4}{3}\pi \left(\frac{A^{in}}{4\pi}\right)^{3/2}}$$

reduced area difference

$$\Delta a := \frac{\Delta A}{8\pi d \left[A^{in}/4\pi\right]}$$

$\Rightarrow$ v - Δa - phase diagram of shapes with minimum bending energy

show fig 12

- Temperature induced shape transitions

$T \uparrow \Rightarrow$ A increases, V = const $\Rightarrow v \downarrow$

$\Rightarrow \alpha^{ex} = \frac{1}{A^{ex}} \frac{dA^{ex}}{dT} = (1+x)\alpha^{in} \Rightarrow \Delta a \uparrow \sigma \downarrow$

show Fig 2, Fig 3, Fig 4

Endocytosis and Exocytosis

show figure

Lipid Tethers:

show figure

- Imre Derényi et al, Formation and Interaction of Membrane Tubes, PRL, Vol 88, 2002

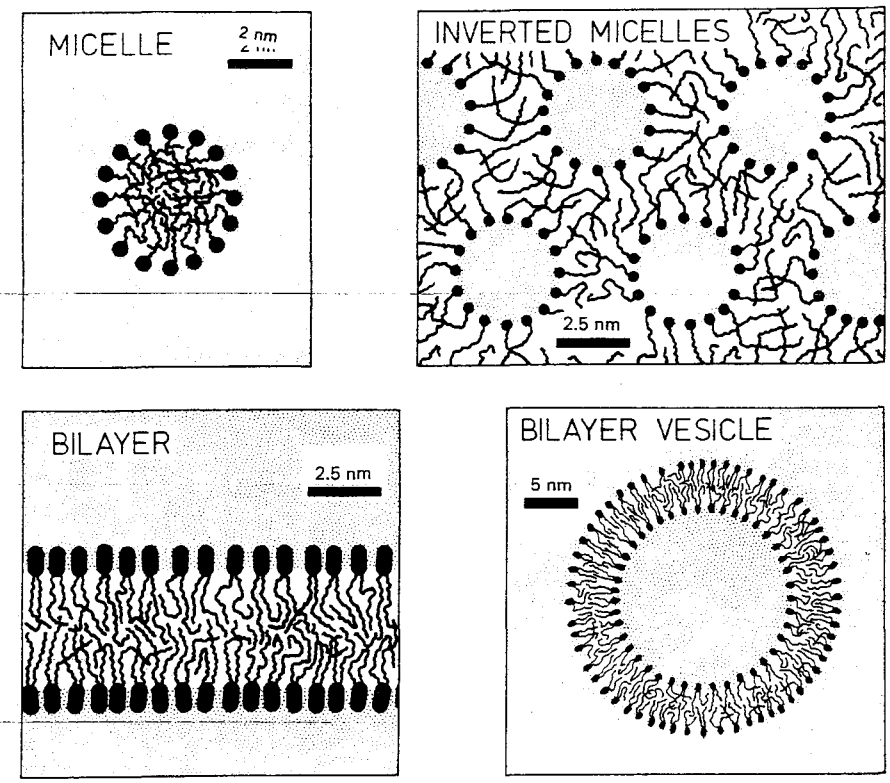

Fig. 16.1. Amphiphiles such as surfactants and lipids (see Table 16.1) can associate into a variety of structures in aqueous solutions. These can transform from one to another by changing the solution conditions such as the electrolyte or lipid concentration, pH, or temperature. In most cases the hydrocarbon chains are in the fluid state allowing for the passage of water and ions through the narrow hydrophobic regions, e.g., across bilayers. The lifetime of water molecules in lecithin vesicles is about 0.02 s, while ions can be trapped for much longer times, about 8 h for Cl^- and one month for Na^+ ions. Most single-chained surfactants form micelles, while most double-chained surfactants form bilayers, for reasons that are discussed in Chapter 17.

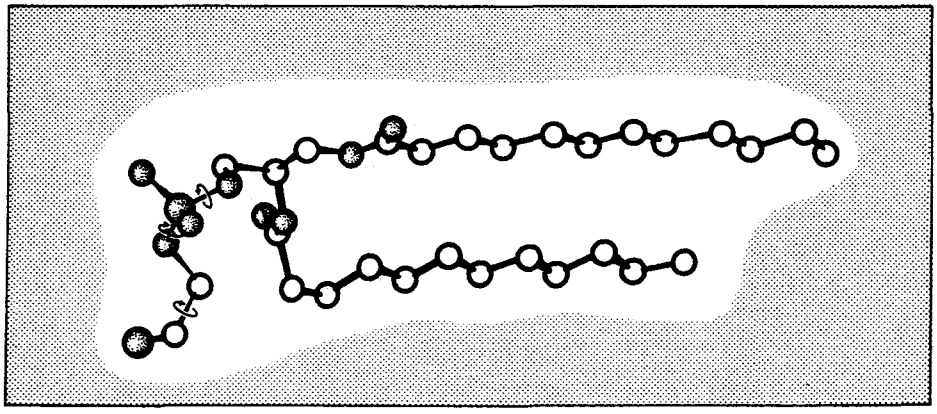

Fig. 16.2. The zwitterionic phospholipid dilauryl-phosphatidyl-ethanolamine containing two saturated hydrocarbon chains and a polar (hydrophilic) headgroup (see also Table 16.1).

TABLE 17.2 Mean (dynamic) packing shapes of lipids and the structures they form

Lipid	Critical packing parameter $v/a_0 l_c$	Critical packing shape	Structures formed
Single-chained lipids (surfactants) with large head-group areas: *SDS in low salt*	$< 1/3$	Cone 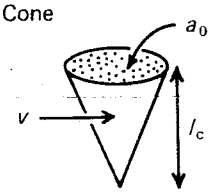	Spherical micelles 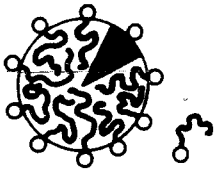
Single-chained lipids with small head-group areas: *SDS and CTAB in high salt, nonionic lipids*	1/3-1/2	Truncated cone 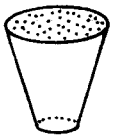	Cylindrical micelles 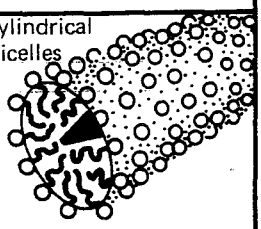
Double-chained lipids with large head-group areas, fluid chains: *Phosphatidyl choline (lecithin), phosphatidyl serine, phosphatidyl glycerol, phosphatidyl inositol, phosphatidic acid, sphingomyelin, DGDG[a], dihexadecyl phosphate, dialkyl dimethyl ammonium salts*	1/2-1	Truncated cone 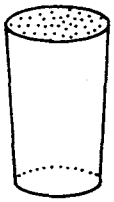	Flexible bilayers, vesicles 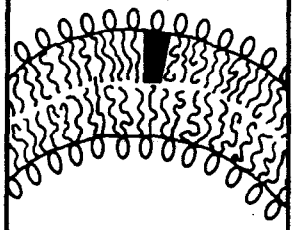
Double-chained lipids with small head-group areas, anionic lipids in high salt, saturated frozen chains: *phosphatidyl ethanolamine, phosphatidyl serine + Ca^{2+}*	~1	Cylinder 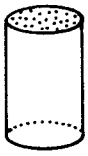	Planar bilayers 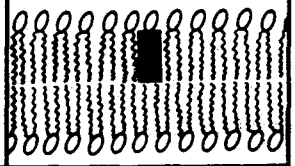
Double-chained lipids with small head-group areas, nonionic lipids, poly *(cis)* unsaturated chains, high T: *unsat. phosphatidyl ethanolamine, cardiolipin + Ca^{2+} phosphatidic acid + Ca^{2+} cholesterol, MGDG[b]*	> 1	Inverted truncated cone or wedge 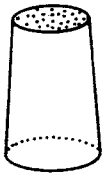	Inverted micelles 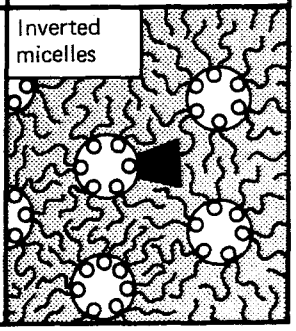

[a] DGDG, digalactosyl diglyceride, diglucosyl diglyceride.
[b] MGDG, monogalactosyl diglyceride, monoglucosyl diglyceride.

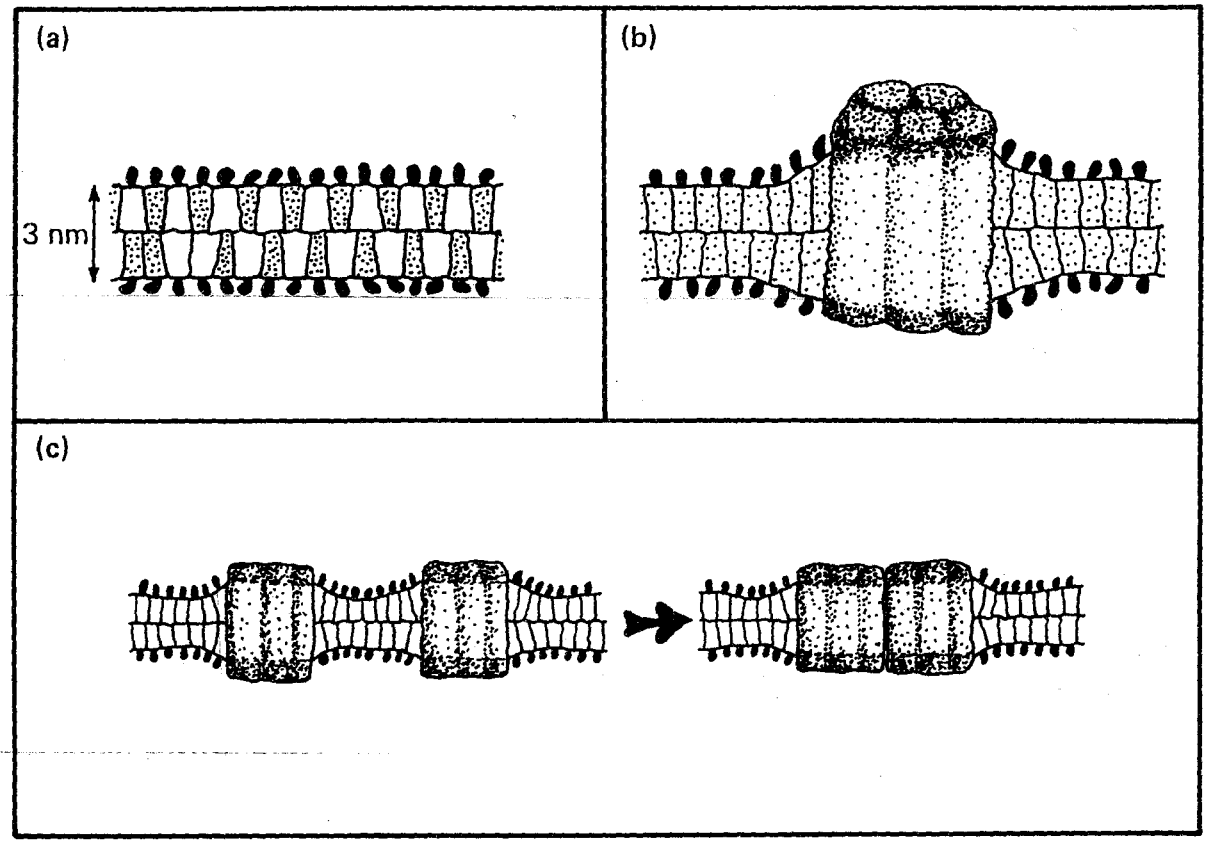

Fig. 17.7. (a) Mixture of two different lipids packing together within a planar membrane. The shaded lipids are cone-shaped ($v/a_0 l_c < 1$); the white lipids are wedge-shaped ($v/a_0 l_c > 1$). (b) Packing constraints induced in the hydrocarbon chain regions of lipids around a protein molecule, which may be relaxed when proteins aggregate, as shown in (c).

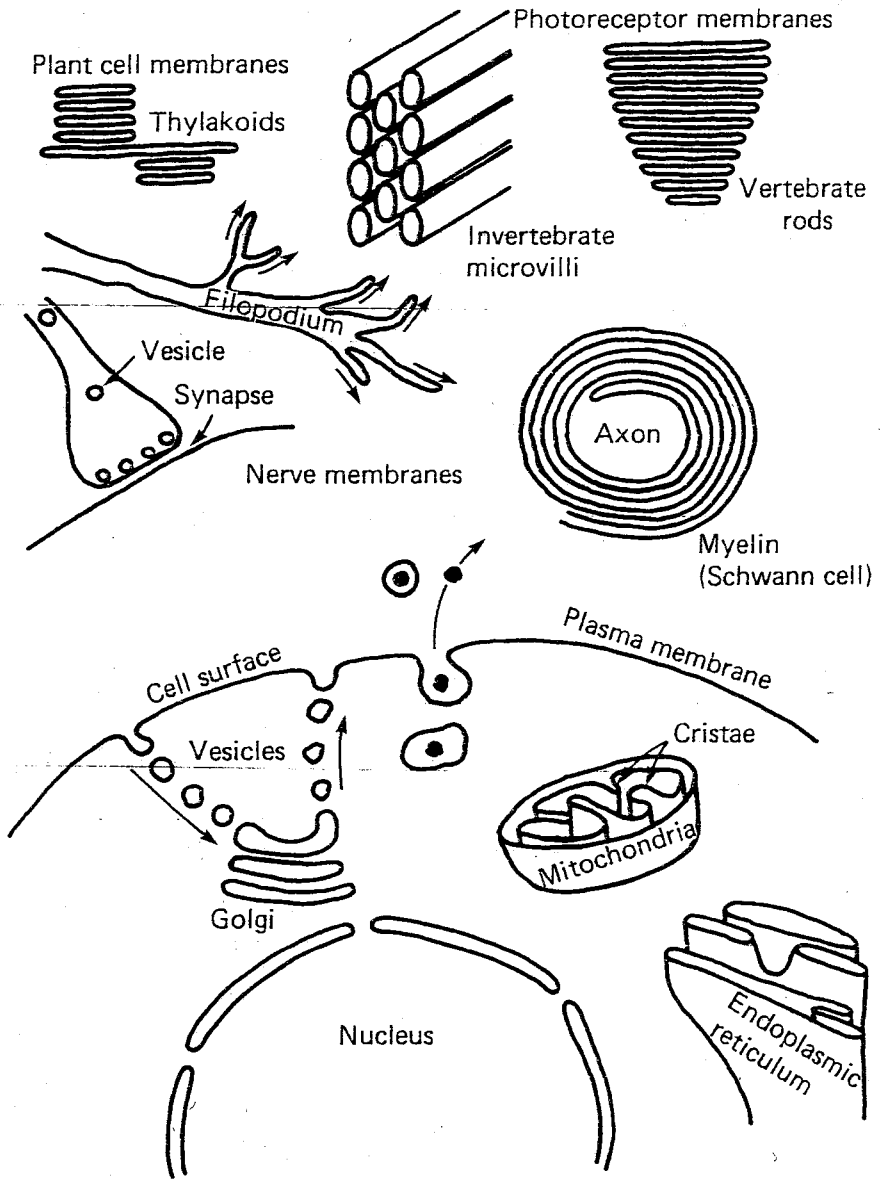

Fig. 17.6. Cellular membranes are thin sheets of lipids and proteins. Most biological membranes offer little resistance to bending.

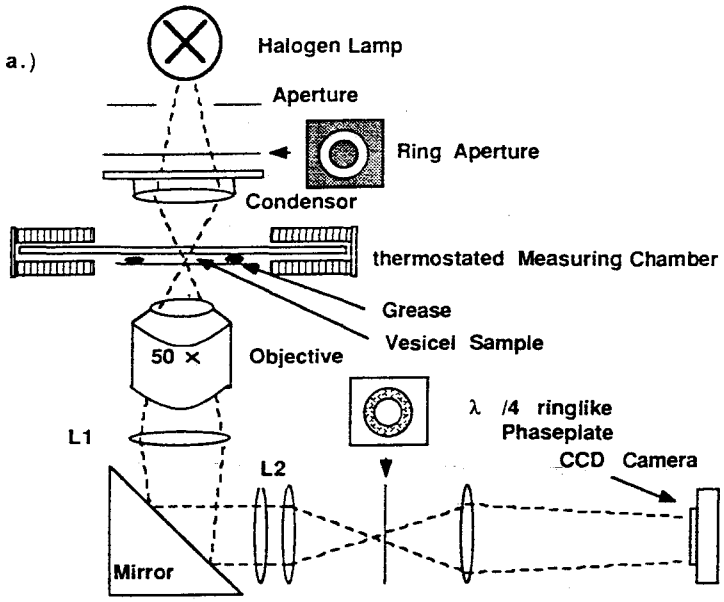

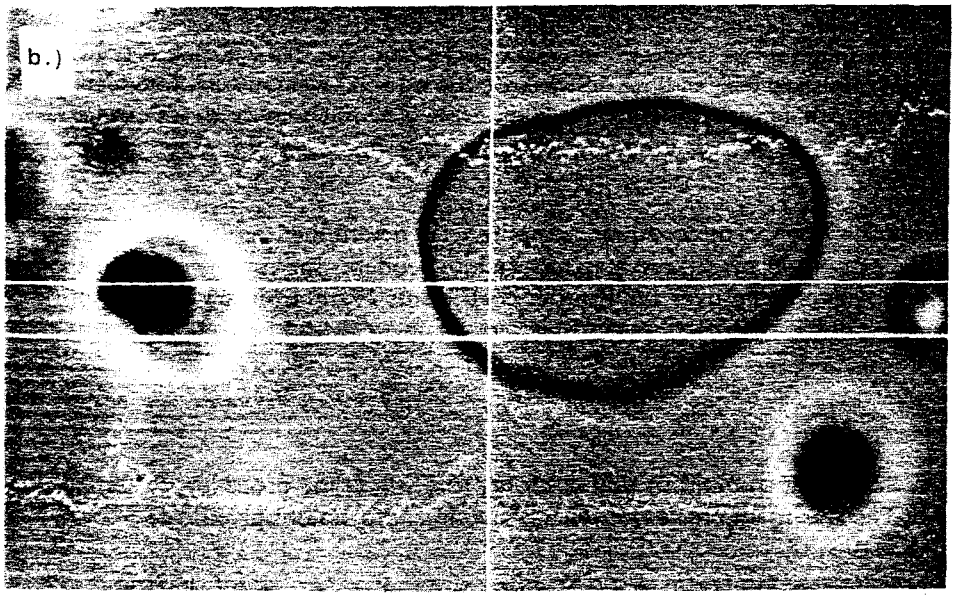

Fig. 1. — a) Schematic view of apparatus built around a inverted Zeiss Aximat microscope used for observation of vesicle. Since the focus of the objective is set at infinity its image plane can be positioned at will by using the lenses L_1 and L_2 and the mirror. Therefore a normal bright field objective (Here : Zeiss 50 ×, Air, Pol, numerical aperture 0.95, working distance 300 μm) can be used for phase contrast microscopy by placing a (ring-like) phase plate in the image plane. The sample could be illuminated with a 100 Watt halogen lamp (Zeiss) or a high pressure mercury lamp (HBO-100) with ultraviolett cut-off filter which improved the optical resolution. b) DMPC-vesicle with intensity distribution (white shaky curve) along a direction indicated by the white straight line. The positions of the contour is determined by the two minima in the intensity distribution.

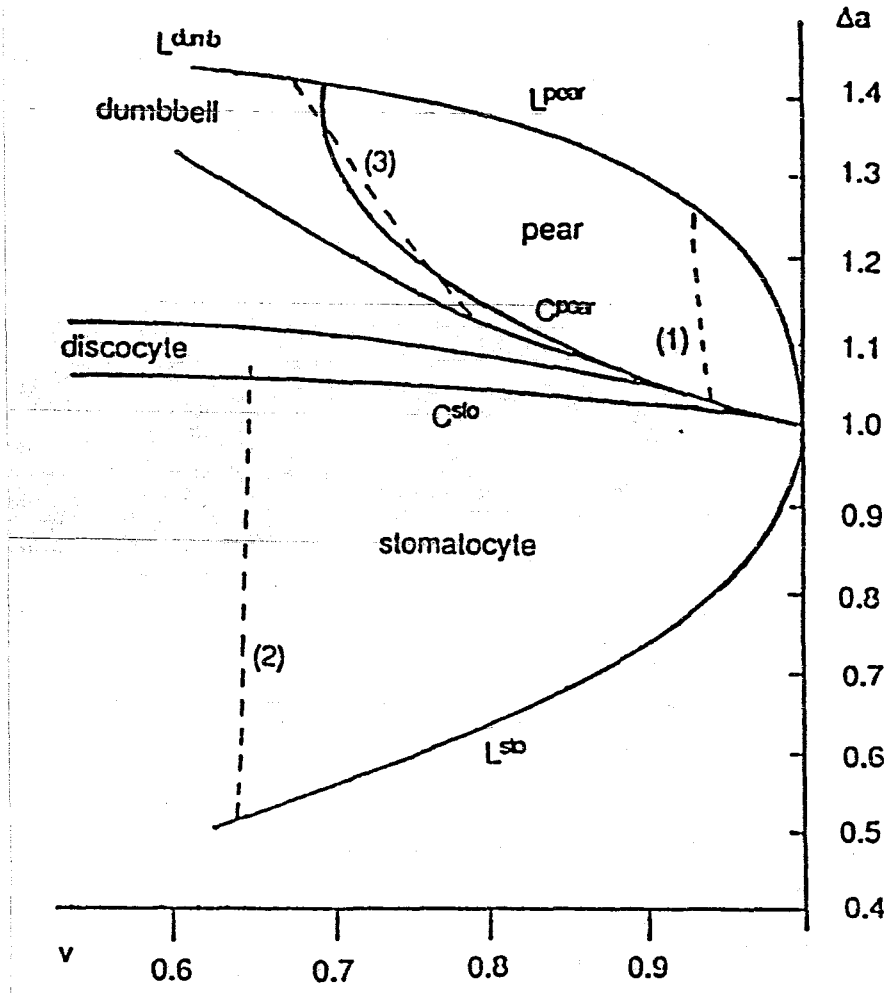

FIGURE 12 Phase diagram of minimum bending energy vesicle shapes calculated by the bilayer coupling approach (8) as a function of the reduced volume, v, and area difference, Δa, between inner and outer monolayer. The phase boundaries denoted by C^{sto}, C^{pear} define two continuous transitions at which the up-down symmetry is broken and the outer solid lines L^{pear}, L^{dumb}, L^{sto} define limiting shapes. Note that for large v values the dumbbell regime contains prolate ellipsoids and the discocyte regime contains oblate ellipsoids. The dashed lines show experimentally observed trajectories which can be described by Eq. 5 for various values of γ (1: $v_0 = 0.94$, $\Delta a_0 = 1.03$, $\gamma = 0.057$, $b = 1500$; 2: $v_0 = 0.65$, $\Delta a_0 = 1.03$, $\gamma = -0.29$, $b = 1000$; 3: $v_0 = 0.78$, $\Delta a_0 = 1.15$, $\gamma = 0.0017$, $b = 640$).

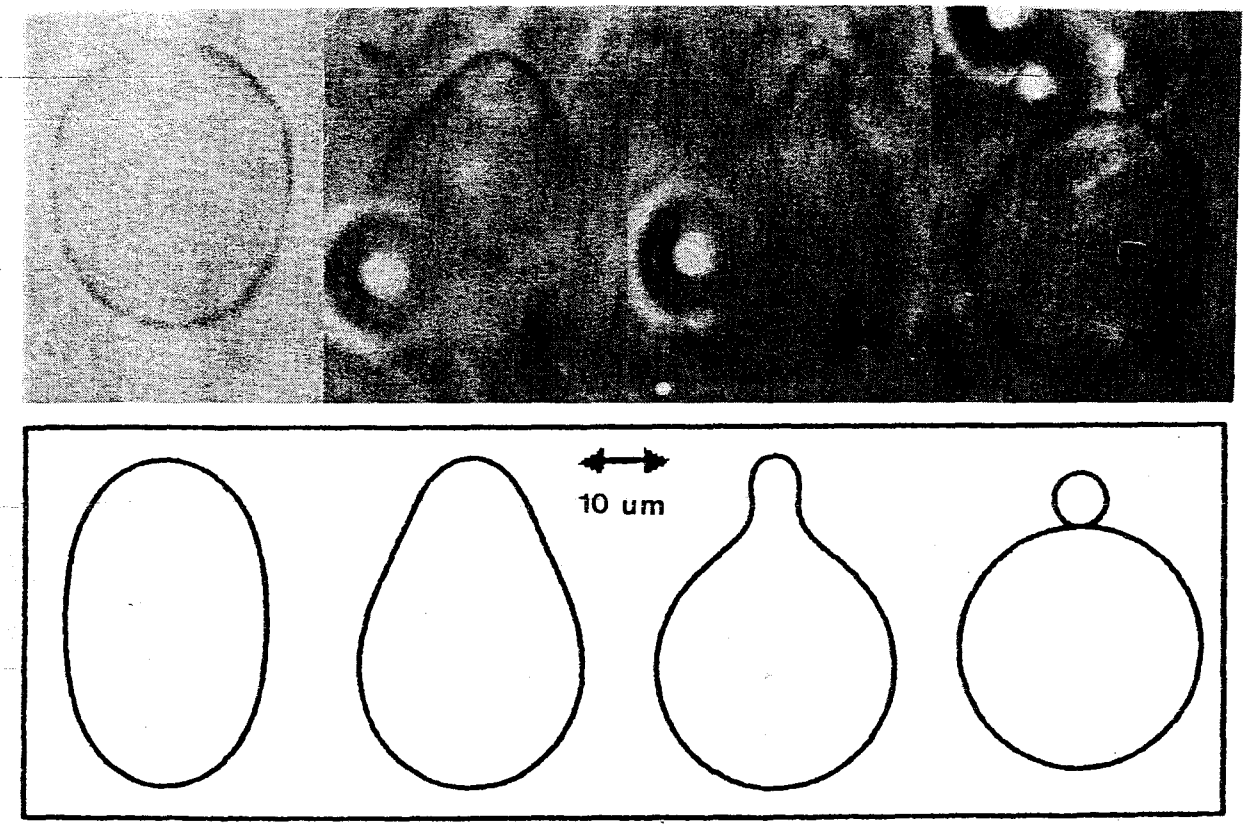

Fig.2. Demonstration of a budding transition: The shapes were measured at T = 31.4, 35.5, 35.6 and 35.8^{0}C. The disc-like object is due to an air bubble which migrates in the outer compartment of the measuring chamber. The calculated shapes correspond to a trajectory of Eqs.(4) with initial values of the reduced volume v_0 = 0.9446 and reduced area difference Δa_0 = 1.0305, γ = 0.057 and b = 1500.

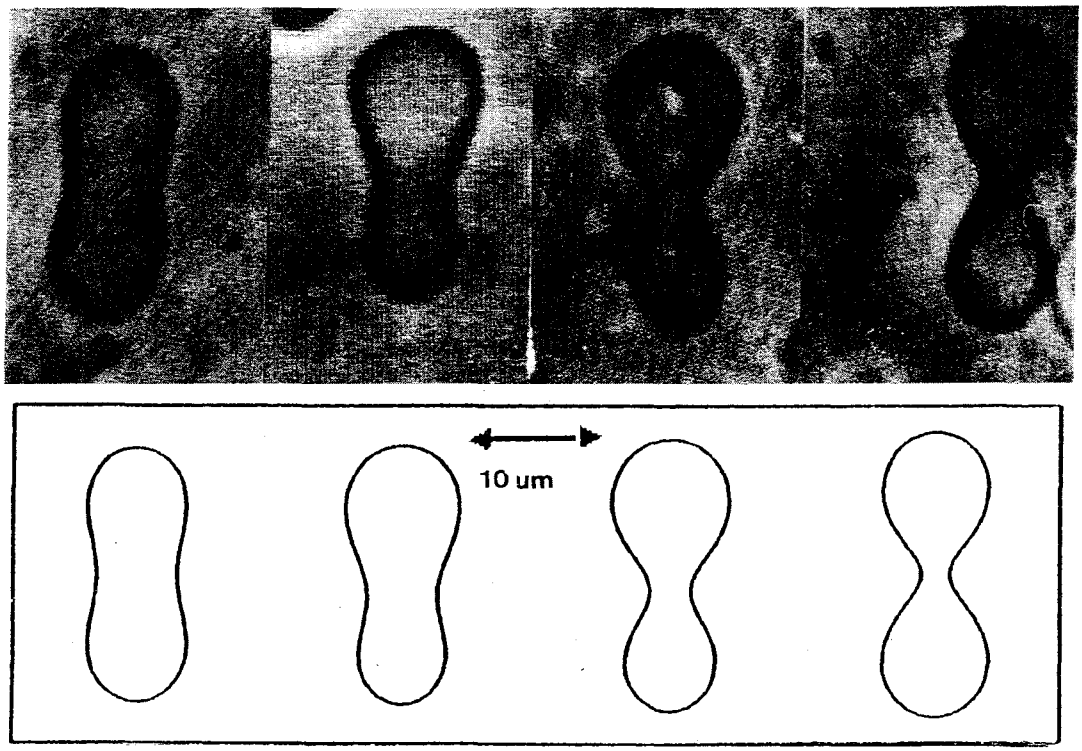

Fig.3. Symmetric-asymmetric reentrant transition: The shapes were measured at T = 30.7, 32.6, 40.0 and 44.3^{0}C. The calculated shapes correspond to a trajectory of Eqs.(4) with υ_0 = 0.78, Δa_0 = 1.1475, γ = 0.00166 and b = 640.

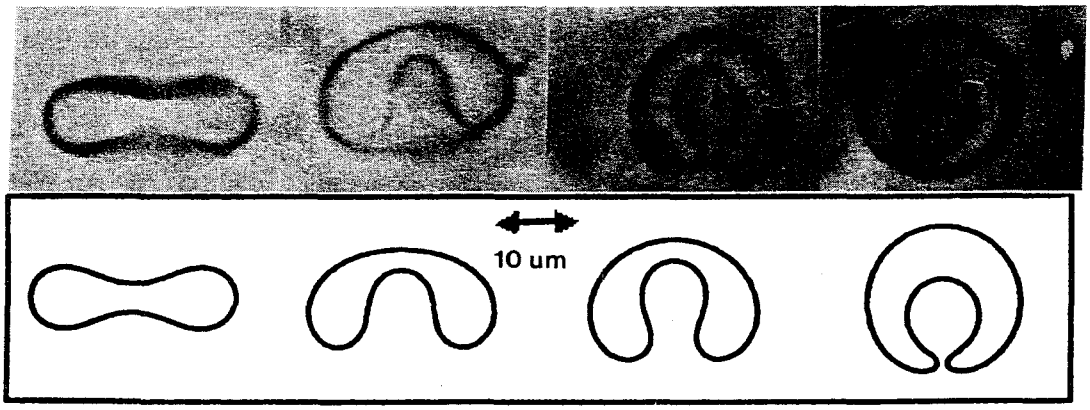

Fig.4. Discocyte-stomatocyte transition: The shapes were measured at T = 43.8, 43.9, 44.0 and 44.1^{0}C. The calculated shapes correspond to a trajectory of Eqs.(4) with υ_0 = 0.65, Δa_0 = 1.0355, γ = -0.29 and b = 1000.

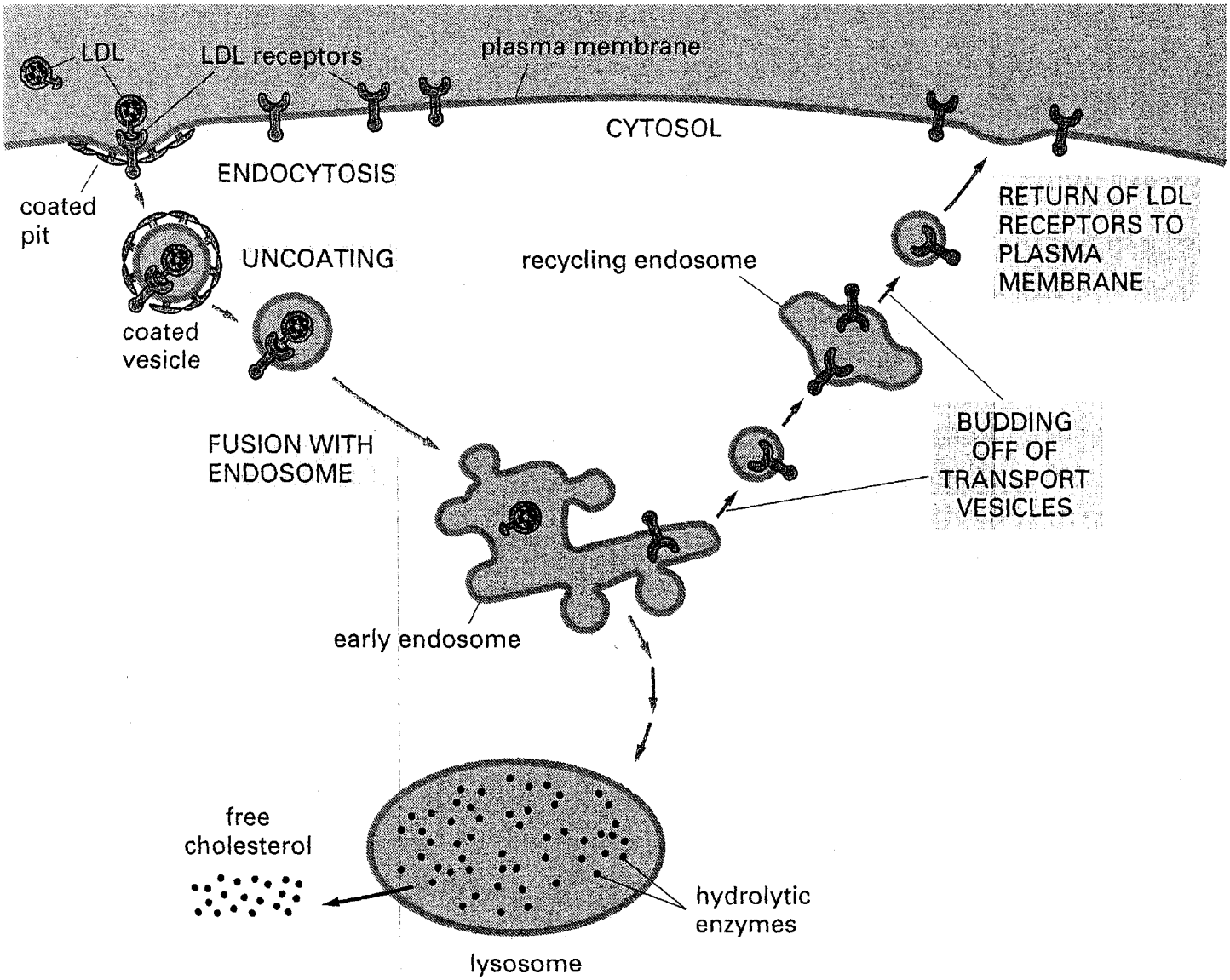
LDL
LDL receptors
plasma membrane
CYTOSOL
ENDOCYTOSIS
coated pit
UNCOATING
coated vesicle
recycling endosome
RETURN OF LDL RECEPTORS TO PLASMA MEMBRANE
FUSION WITH ENDOSOME
BUDDING OFF OF TRANSPORT VESICLES
early endosome
free cholesterol
hydrolytic enzymes
lysosome

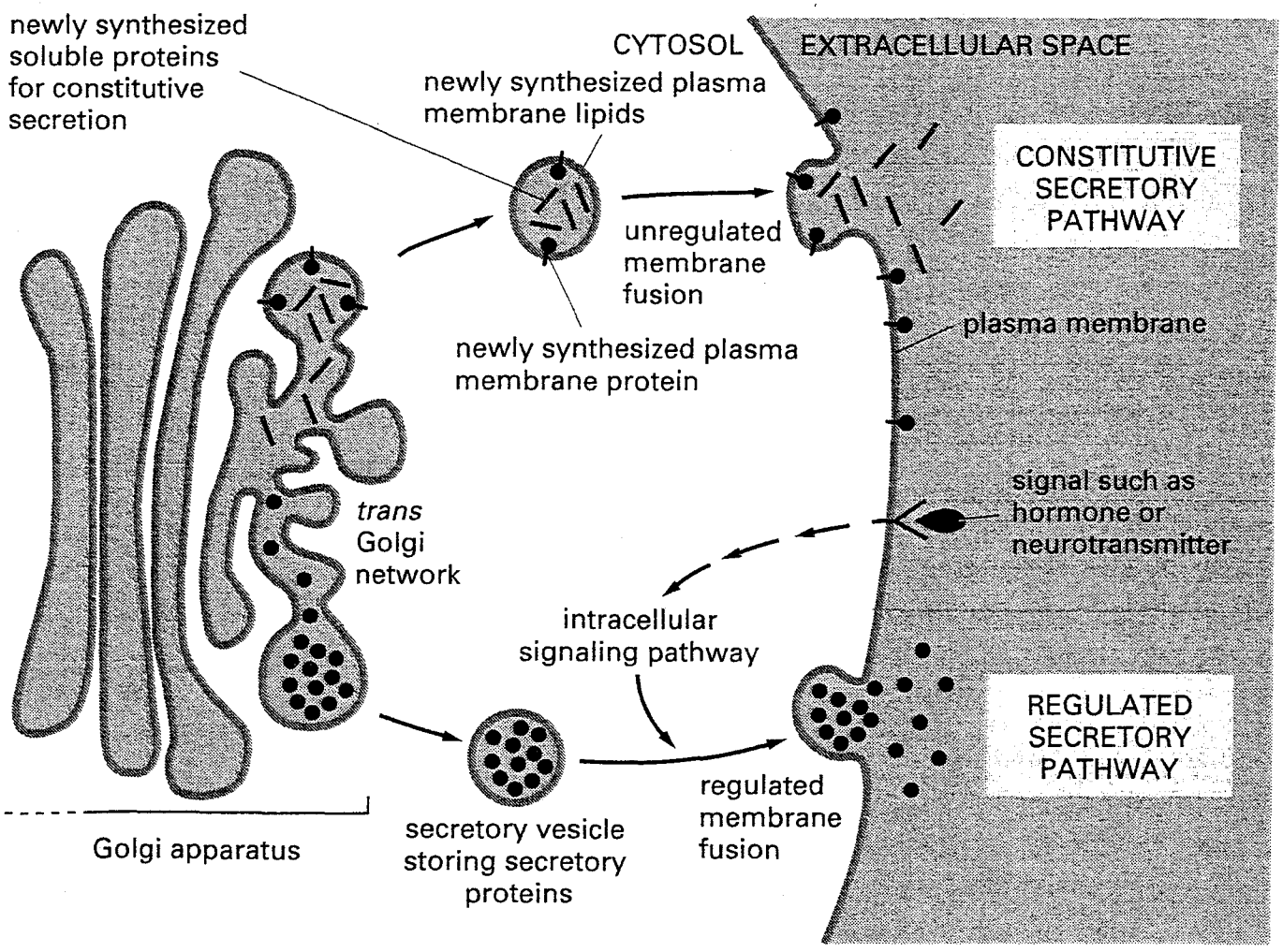
newly synthesized soluble proteins for constitutive secretion
CYTOSOL
EXTRACELLULAR SPACE
newly synthesized plasma membrane lipids
CONSTITUTIVE SECRETORY PATHWAY
unregulated membrane fusion
plasma membrane
newly synthesized plasma membrane protein
signal such as hormone or neurotransmitter
trans Golgi network
intracellular signaling pathway
REGULATED SECRETORY PATHWAY
regulated membrane fusion
secretory vesicle storing secretory proteins
Golgi apparatus

Fig. 4
Membrane tubes pulled out by molecular motors (kinesins). a) The minimal system we have used b) Membrane tubes Networks pulled out a vesicle using the system a). Fluorescent lipids have been incorporated into the membranes in order to obtain these images with a confocal microscope. (bar : 5 µm)

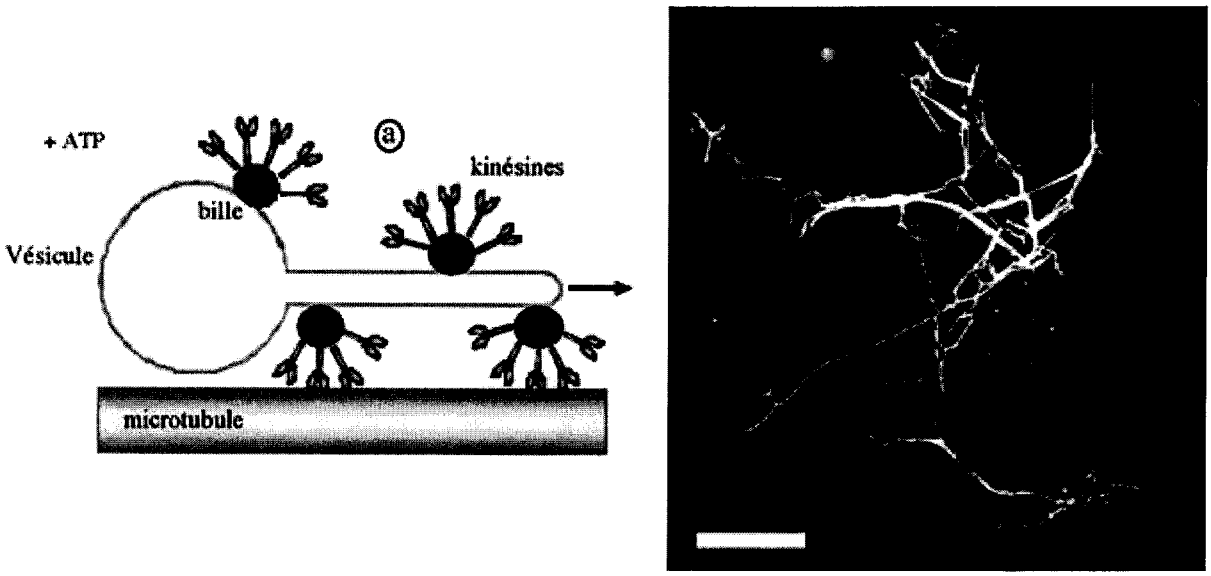

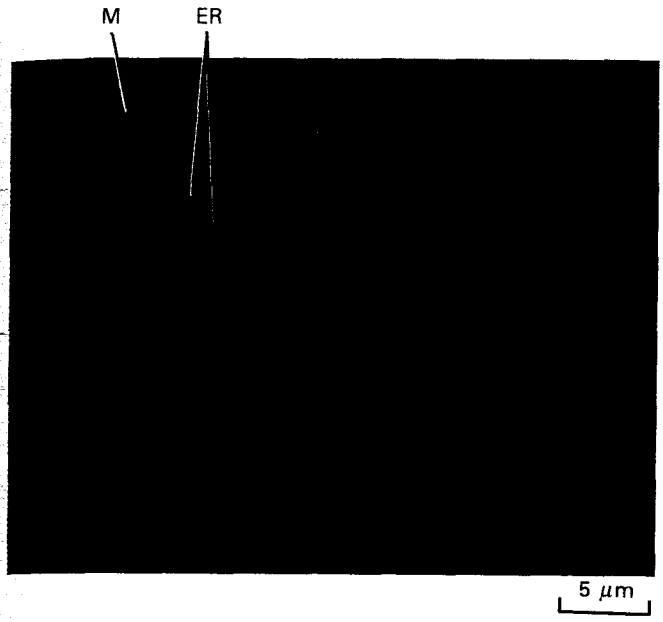

◀ FIGURE 5-11 Fluorescence micrograph of the endoplasmic reticulum (ER) in a flattened region of a living monkey kidney epithelial cell. The ER is a set of elongated membrane vesicles fibers that fuse with each other to form a network, or reticulum. The larger, nonreticular fluorescent structures are mitochondria (M). [See C. Lee and L. B. Chen, 1988. *Cell* **44**:37–46. Courtesy of L. B. Chen.]

Fluorescence Microscopy Can also Measure the Local Concentration of Ca^{2+} Ions and the Intracellular pH

Changes in the cytosolic concentration of Ca^{2+} ions or pH will frequently signal changes in cellular metabolism. The Ca^{2+} concentration in the cytosol of resting cells, for instance, is about 10^{-7} M. Many hormones or other stimuli frequently cause a rise in Ca^{2+} to 10^{-6} M; this, in turn, causes changes in cellular metabolism, such as contraction of muscle, as is described in Chapter 20. The fluorescent properties of certain dyes, such as *fura-2* (Figure 5-12),

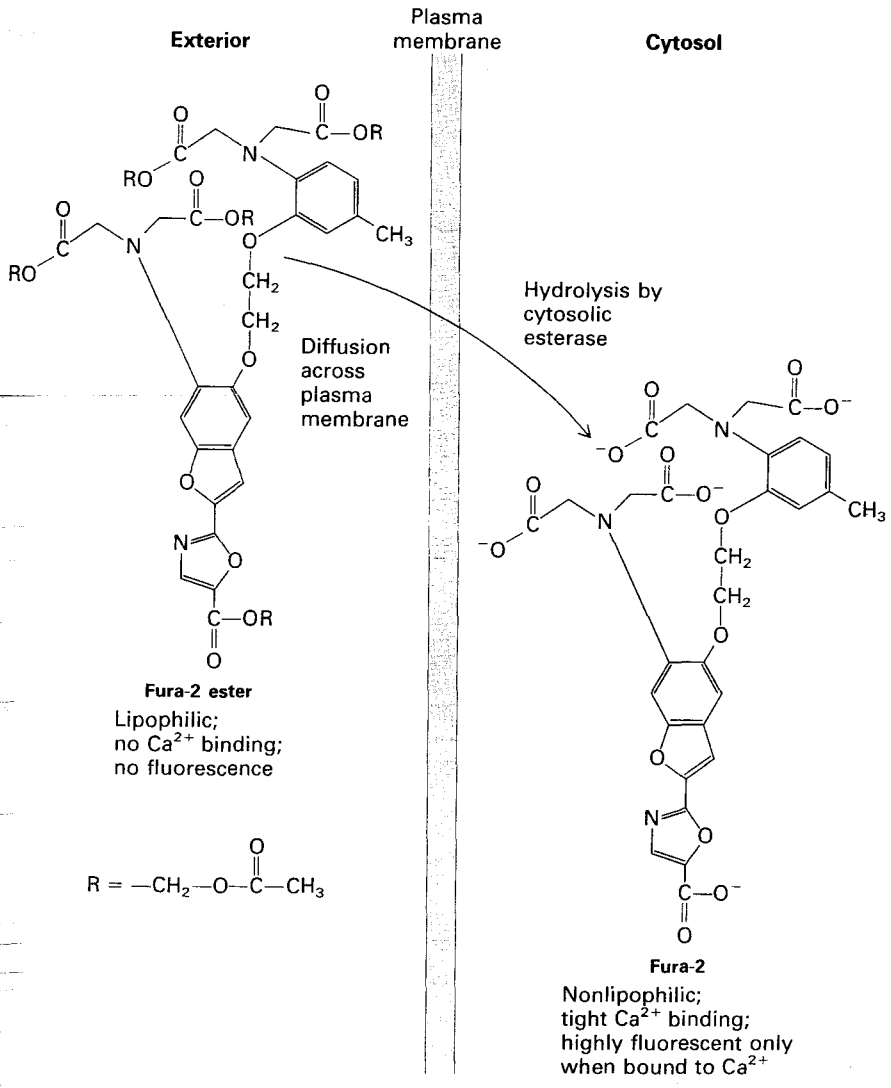

◀ FIGURE 5-12 The cytosolic concentration of Ca^{2+} can be monitored continuously by the fluorescence of Ca^{2+}–fura-2 complexes. When added to a medium, the lipophilic fura-2 ester (*left*) diffuses across the plasma membrane and is hydrolyzed to fura-2 by cytosolic esterases. Nonlipophilic fura-2 (*right*) cannot cross cellular membranes and remains in the cytosol. Fura-2 is not fluorescent unless Ca^{2+} is present, and the fluorescence of Ca^{2+}–fura-2 complexes is proportional to the concentration of Ca^{2+} ion in the cytosol.